Analytical Expression for the Impact of Velocity Variations on Azimuth Ambiguity Suppression in Digital Beamforming SAR

Luiz Fernando Quandt Fusinato[a], Juan Pablo Navarro Castillo[a], and Rolf Scheiber[a]
[a]German Aerospace Center (DLR), Microwaves and Radar Institute, Münchener Str. 20, 82334 Oberpfaffenhofen, Germany

Abstract

Airborne SAR demonstrators are employed to validate digital beamforming (DBF) techniques and support the development of high-resolution wide-swath (HRWS) operational modes for spaceborne SAR missions. These systems process data from multiple apertures displaced in azimuth using a bank of reconstruction filters based on signal models. However, the models have to assume a constant velocity, which does not hold in airborne SAR systems. The focus of this work is to develop an analytical expression to predict the impact of velocity variations on the suppression of azimuth ambiguities. The proposed expression provides an analytical prediction of the azimuth ambiguity-to-signal ratio (AASR) as a function of the velocity error. The expression is validated using point target simulations. Finally, its potential application to estimate an optimal reconstruction block size is discussed and evaluated.

1 Introduction

A typical limitation of SAR systems operating in stripmap mode is the compromise between high azimuth resolution and wide swath [1]. The use of digital beamforming (DBF) presents a solution to this problem through the use of multiple receive apertures displaced in the along-track direction, each operating at a low pulse repetition frequency (PRF). This configuration will be adopted in future high-resolution wide-swath (HRWS) SAR missions, such as ROSE-L [2], to overcome this limitation. By definition, the system PRF in HRWS SAR sensors will be smaller than the required processed azimuth bandwidth, leading to aliasing in the Doppler spectrum. Consequently, each channel cannot be processed independently, as this would cause azimuth ambiguities to appear in the respective focused SAR image. This problem is solved by a bank of reconstruction filters that combine the information from the different channels, resulting in a unambiguous SAR signal with an effective PRF higher than the original.

Between the different proposed algorithms for the reconstruction, a well-known approach is the matrix inversion method, as presented in [1]. This technique models the impulse response function (IRF) for each channel based on the geometry and velocity of the SAR sensor. Using this information a system matrix is built and inverted to obtain the values for the respective reconstruction filters. One of the considerations adopted by the definition of the model is the assumption of constant velocity during the flight, which does not apply in airborne SAR sensors.

One of the solutions to deal with velocity variations is to divide the acquisition along the azimuth track in blocks and calculate an average velocity for each one of them to be used in the filter computation, as proposed in [3]. One important step in this approach is the selection of the block size, which must be small enough to ensure that velocity variations are negligible for an effective suppression of ambiguous power, but large enough to provide sufficient frequency resolution and reduce computational cost [3].

To estimate an optimal block size, a relationship between performance and velocity variation is required to determine the maximum allowable velocity deviation within a processing block. This can be done, for instance, by running a big amount of point target simulations varying progressively the block size and computing the azimuth ambiguity-to-signal ratio (AASR), as shown in [3]. Nevertheless, this process is tedious and not computationally efficient. In [4], a model describing the phase error as a function of the velocity deviation is presented. However, it only provides an indirect relation between velocity variation and the actual ambiguity suppression.

This work proposes a more efficient way to directly compute the AASR as a function of the velocity variation by redefining the analytical expression first presented in [5,6], which estimates analytically the AASR using the signal model and the reconstruction matrix. This new expression could be used to define the maximum acceptable velocity variation needed to guarantee a chosen maximum ambiguity level, optimizing the step of defining the block size during the aforementioned method, without the need of a test and trial method.

This paper is organized as follows: Section 2 provides context through the DBF system model, the theory around the reconstruction algorithm and the AASR calculation. Section 3 presents the model for the velocity variation and the development of the analytical expression. Section 4 compares the results from simulations and the expression. Finally, Section 5 concludes this work.

2 Theoretical Background

In this section, the relevant elements required to develop the expression proposed in this paper, as well as the traditional way to calculate analytically the AASR are presented.

2.1 Multichannel Signal Model

The reception of an echo by multiple apertures with different positions along azimuth can be modeled in the frequency domain as a monostatic reference signal $U(f)$ multiplied by a channel-dependent component $H_j(f)$ [1]. Consequently, the signal at receiver j can be expressed as

$$U_j(f) = H_j(f) \cdot U(f) = H_j(f) \cdot H_s(f) \cdot U_s(f) \quad (1)$$

where $U_s(f)$ represents the reflectivity of the scene and $H_s(f)$ the conventional monostatic SAR impulse response [5]. As introduced in [1], in single platform DBF SAR systems, $H_j(f)$ can be approximated by a constant phase term and a time-shift as a function of the distance between the transmitter and the respective receiver in the azimuth direction (Δx_j). The model is illustrated in **Figure 1**. $H_j(f)$ can be then expressed as

$$H_j(f) = exp\left[-i \cdot \frac{\pi \Delta x_j^2}{2 \cdot \lambda \cdot r_0}\right] \cdot exp\left[-i \cdot 2\pi \cdot f \cdot \frac{\Delta x_j}{2 \cdot v_0}\right] \quad (2)$$

where λ is the wavelength of the signal, r_0 is the slant range, v_0 is the assumed aircraft velocity and f is the Doppler frequency.

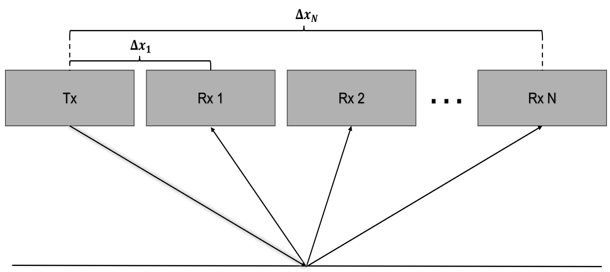

Figure 1 Diagram representing the geometry of a DBF SAR system with one single transmitter and multiple receivers separated in azimuth.

Using (2) for each channel and PRF subband, the reception can be modeled by the matrix $H(f)$, where each column represents a different channel and each row represents a different subband. The interval $f \in \left[-\frac{N \cdot PRF}{2}, -\frac{N \cdot PRF}{2} + PRF\right]$ represents the lowest subband, where N indicates the number of channels. The other subbands are represented by shifting the frequency interval by an integer number of PRF:

$$H(f) = [\gamma_1(f) \; ... \; \gamma_N(f)] \quad (3)$$

where each element $\gamma_j(f)$ is a column vector and can be defined as

$$\gamma_j(f) = \begin{pmatrix} H_j(f) \\ H_j(f + PRF) \\ \vdots \\ H_j(f + (N-1) \cdot PRF) \end{pmatrix} \quad (4)$$

2.2 Azimuth Reconstruction

When $H(f)$ is inverted, it defines the filters used for the reconstruction of the signal through the matrix $P(f)$. Each filter $P_{jm}(f)$ is associated to a channel j and a subband m.

$$P(f) = H^{-1}(f) \quad (5)$$

This way, if the velocity is constant and it matches the value used to define $H(f)$, the filters defined using the matrix $P(f)$ should be able to perfectly reconstruct the range-compressed signal, with a new effective azimuth sampling frequency of $N \cdot PRF$ [1]. The reception of the signal followed by the reconstruction is represented in **Figure 2**.

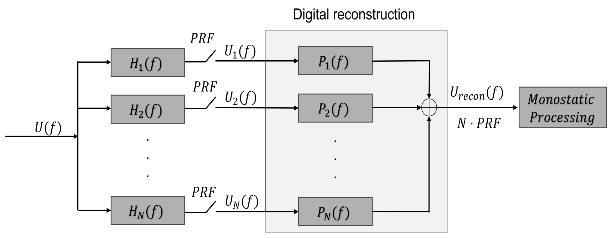

Figure 2 Diagram representing the reception model and the algorithm for the digital reconstruction of the signal.

2.3 Traditional AASR Estimation

According to [5,6], the AASR can be calculated by adding the ambiguous energy located outside the reconstruction bandwidth after it is processed by the filters. Defining the monostatic SAR signal by $U_0(f_D) = U(f_D)$, and its replicas by $U_k(f_D) = U(f_D + k \cdot PRF)$ it is possible to calculate the term $e_\Sigma(f_D)$, related to the ambiguous energy:

$$e_\Sigma(f_D) = \sum_{\substack{k=-\infty \\ k \neq 0}}^{\infty} U_k(f_D) \cdot \sum_{m=1}^{N} \sum_{j=1}^{N} H_{jk}(f_D) \cdot P_{jm}(f_D) \quad (6)$$

where $f_D \in \left[-\frac{N \cdot PRF}{2}, +\frac{N \cdot PRF}{2}\right]$ represents the complete reconstruction bandwidth and $H_{jk}(f_D) = H_j(f_D + k \cdot PRF)$.

Taking the mean over Doppler of the squared absolute value of this term, we have the ambiguous power in azimuth, which, when divided by the original signal power p_s, results in the AASR.

$$AASR = \frac{\overline{|e_\Sigma(f_D)|^2}}{p_s} \quad (7)$$

Nevertheless, this method assumes the ambiguous energy within the reconstruction bandwidth to be completely suppressed, which does not happen, if there are deviations from the model used to define the matrix $H(f)$.

3 AASR Estimation for Cases with Velocity Mismatch

The expression proposed in this section complements the definition in (6) by estimating the residual ambiguous energy within the reconstruction bandwidth when the model has errors. More specifically, this work focuses on the impact of deviations from the nominal velocity used to determine the channel-dependent time shift in (2).

3.1 Proposed Error Model

In order to study the ambiguities that appear from the mismatch between the aircraft velocity and the one used to compute $P(f)$, a constant difference between them (Δv) was considered and the effect of the channel is now given by:

$$\hat{H}_j(f) = exp\left[-i \cdot \frac{\pi \Delta x_j^2}{2\lambda r_0}\right] exp\left[-i \cdot 2\pi f \frac{\Delta x_j}{2(v_0 + \Delta v)}\right] \tag{8}$$

Moreover, the equivalent monostatic SAR signal $U(f)$ needs to be rewritten as $\hat{U}(f)$ since the real sensor's velocity is present not only in $H_j(f)$, but also in the definition of the conventional monostatic impulse response $H_s(f)$ [5]. Adapting every term of the matrix $H(f)$ to include this velocity deviation, it is possible to define a new system matrix $\hat{H}(f)$. By performing the matrix multiplication of $P(f)$ and $\hat{H}(f)$, a new matrix can be defined that serves to evaluate the mismatch between the reconstruction model and the real model of the input multichannel signal:

$$M(f) = \hat{H}(f)P(f) = \hat{H}(f)H^{-1}(f) \tag{9}$$

Each element in the main diagonal of $M(f)$ is related to the desired contribution of the signal in the respective subband. The rest of elements in $M(f)$ are related to the undesired ambiguous contribution in the respective subband. **Figure 3** depicts the power of each overlapped contribution of $\hat{U}(f)$ in each subband after azimuth reconstruction. In an ideal case where $\Delta v = 0$ (blue line), the resulting $M(f)$ should be the unity matrix. This means that in every subband the desired contribution will be multiplied by one and the ambiguous contributions will become zero. However, in the case with a velocity error (orange dotted line), the elements outside of the diagonal are different than zero, representing interferences that the subbands cause on each other's reconstructions, resulting in residual azimuth ambiguities.
Additionally, the elements in the diagonal of $M(f)$ are no longer equal to one. As a consequence, the energy of the desired contribution in each subband will not be perfectly preserved along the reconstruction bandwidth. Nevertheless, in the cases studied in this paper this effect is small and can be considered negligible.

3.2 AASR Expression

Through a similar logic as the one used in [5,6], it is possible to derive an expression to calculate the ambiguous power and consequently the AASR for a reconstruction with velocity error. The main differences now being that the subbands are not perfectly filtered by the $P(f)$ matrix. In this case, the terms from the matrix $M(f)$ outside of the diagonal represent ambiguous energy caused by interferences between subbands, and terms from the diagonal represent how the original signal is slightly suppressed by the reconstruction. Both groups of terms must be considered on different calculation steps. For this work, a bandlimited signal will be considered, in order to keep those effects caused by $M(f)$ as the only source of ambiguity.
For this calculation, the unambiguous energy is related to the sum of each subband of the original signal multiplied by the respective term on the diagonal of $M(f)$:

$$s(f) = \sum_{k=1}^{N} \hat{U}(f + (k-1) \cdot PRF) \cdot M_{kk}(f) \tag{10}$$

The term related to the ambiguous energy is given by all terms outside of the diagonal, or by the sum of the whole matrix subtracted by the diagonal terms:

$$e(f) = \left(\sum_{m=1}^{N} \sum_{k=1}^{N} \hat{U}(f + (k-1) \cdot PRF) \cdot M_{km}(f)\right) - s(f) \tag{11}$$

Then, the expression to estimate the AASR can be derived by averaging the square of those terms over Doppler:

$$AASR = \frac{\overline{|e(f)|^2}}{\overline{|s(f)|^2}} \tag{12}$$

Finally, it is important to remark that this expression calculates the AASR resulting from the mismatch between the reconstruction model and the real signal model within the reconstruction bandwidth, but does not include the residual ambiguous energy defined outside this bandwidth (see Section 2.3). In order to generalize the analytical expression of the AASR for a DBF SAR system both the method

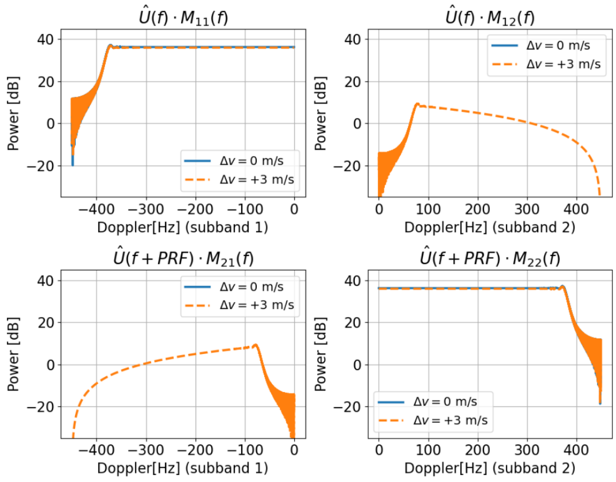

Figure 3 Power of each overlapped contribution in every subband after reconstruction. Simulation of a DBF SAR system with two channels and a velocity error of Δv.

introduced in [5,6] and the one presented in this paper have to be combined, but this is out of scope in the present work.

4 Simulation and Results

In order to test the efficiency of the expression to predict AASR for different errors in velocity, two different simulations were used: a 1-D simulation to compare the AASR results for a multitude of velocity errors, and a 2-D simulation to test the equation on the process of deciding the block size on a block processing algorithm given a certain ambiguity threshold.

For both cases, the parameters of the simulations were used as input for the analytical expression, together with a vector of velocity offsets. The case with a constant velocity error was used as it tends to be the worst case scenario, leading to the highest AASR values and serving as a safer although pessimistic estimate.

4.1 1-D Simulations

The geometry and parameters used in the simulations are chosen based on the geometry of the DLR's DBFSAR demonstrator [7,8], and are listed in **Table 1**.

PRF	450 Hz
Number of Channels	2
Average velocity	90.2 m/s
Wavelength	0.031 m/s
r_0	3134 m
Time of illumination	5.1 s
distance between receivers	0.2 m
Bandwidth (B_{az})	855 Hz

Table 1 Parameters used for the 1-D simulation.

For the 1-D simulation, a chirp of a single target is generated to serve as reference, considering a constant error in velocity. This reference signal is subsampled and modified accordingly to each channel to generate an input representing the received signals of a flight with a mismatch between the expected and the effective velocities.

This input is multiplied by the $P(f)$ matrix, which is the inverse of $H(f)$ when calculated using the expected velocity of the aircraft, not the real one. This mismatch between the velocity that generates the input and the one used when modeling the reconstruction matrix will result in ambiguities on the output signal.

To generate the equivalent to $s(f)$ (see (10)) in the point target simulation, we need to scale the reference signal in order to account for the loss of energy preservation in the desired reconstructed signal due to model mismatch. To do this, each subband of the oversampled reference is multiplied by the corresponding element in the diagonal of the matrix M, which was previously defined in the analytical calculation.

The AASR is calculated before focusing, by the summation of the squared absolute values along the whole signal in frequency domain, subtracted by the power of the scaled reference signal's power, and divided by it. This process is repeated for many different velocities.

In order to test the analytical solution, the reference signal generated for the 1-D simulation was used as input for the expression given by (12), together with the parameters from **Table 1**. The comparison between the processes for the simulation and the expression testing are represented by the diagram in **Figure 4**.

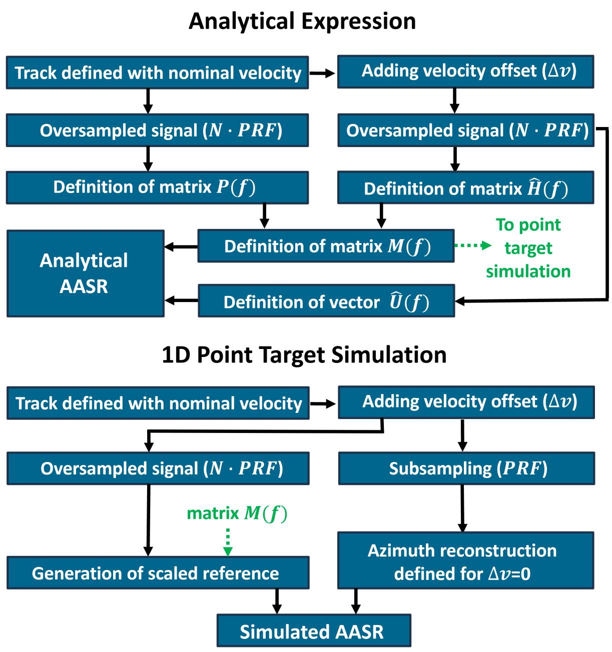

Figure 4 Block diagram summarizing the process to calculate the analytical and simulated AASR presented in this paper.

The results from the expression and from the complete simulation for a range of different velocity offsets is presented in **Figure 5**. The results show a good correspondence, with the exception of cases with really small errors in velocity (lower than 0.1 m/s), where the ambiguity predicted by the equation quickly tends to zero (or $-\infty$ dB).

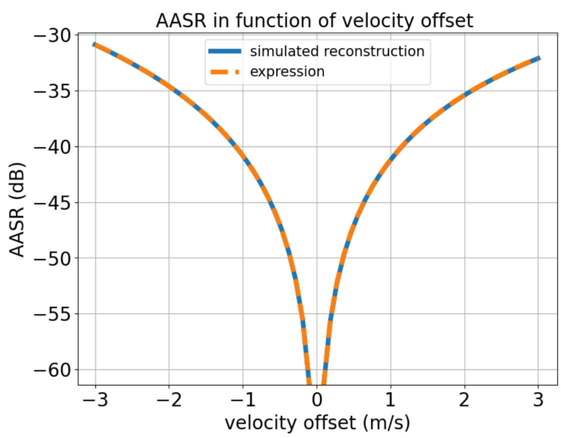

Figure 5 AASR versus velocity error on a 1-D simulation (in blue) or by the analytical prediction (orange).

The signal reconstructed by $P(f)$ can be focused (**Figure 6**) after a velocity interpolation, made by resampling the

signal from being equidistant in time to be equidistant in space.
The effect of extra processing steps like the velocity interpolation are not taken into account by the expression and make the ambiguities lower than the ones predicted by the proposed method. The prediction could be used as a pessimistic estimation of the azimuth ambiguity level after azimuth compression, since the total ambiguous level will be divided into different physical positions.

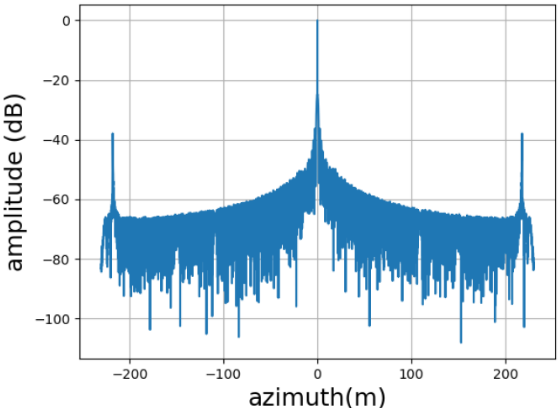

Figure 6 Focused signal of a 1-D simulation, considering a velocity deviation of $-3m/s$.

4.2 2-D Simulations

For the 2-D simulation, a velocity vector measured on a real F-SAR flight was used (the same from [3]), the other parameters are listed on **Table 2**. The AASR was calculated directly from the frequency domain spectrum, before the focusing process.

PRF	150 Hz
Number of Channels	3
Expected velocity	90.2 m/s
Wavelength	0.031 m/s
r_0	3134 m
Time of illumination	2.55 s
distance between receivers	0.4 m
Bandwidth (B_{az})	427 Hz

Table 2 Parameters used for the 2-D simulation.

Many iterations of the processing were made, using different block sizes, and calculating the AASR for each case as shown in **Figure 7**. Then, the parameters of the simulation were used as an input to the analytical expression, considering a constant velocity error (as a worst case scenario).
In **Figure 8**, the results acquired through the expression are shown. Using this plot of AASR versus velocity error, it is possible to define the block size that satisfy a desirable limit for the AASR, avoiding the use of many iterations of full simulations.
For example, if a maximum of $-40dB$ was required, the curve indicates a maximum velocity offset of 0.5 m/s. Comparing with the results from **Figure 7**, this AASR happens for a block size around 750 samples, which is related

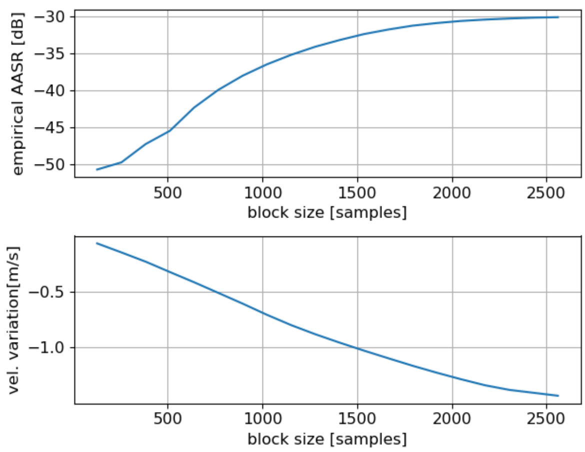

Figure 7 AASR calculated and maximum velocity variation within a single block versus each block size tested on a 2-D simulation.

to a maximum absolute velocity variation of 0.5 m/s. A focused point target from this simulation is represented by **Figure 9**.

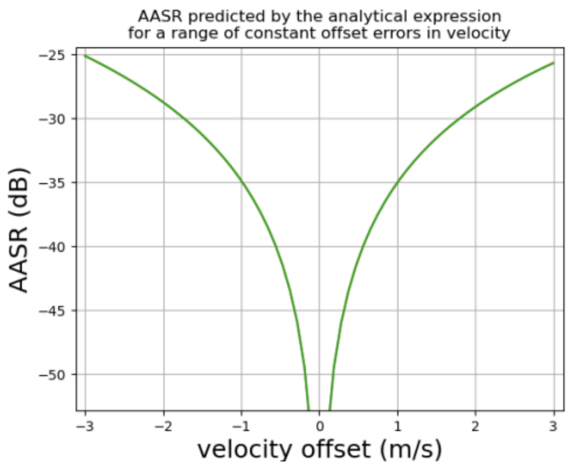

Figure 8 AASR calculated through the analytical expression using the same parameters from the 2-D simulation for a range of different constant velocity errors.

Compared to the 1-D simulation from the previous section, the 2-D simulation has a more complex azimuth process, since it involves a range cell migration correction, a more complex velocity interpolation, and the velocity error is not constant over time anymore. Those extra factors can complicate the correct estimation of the residual ambiguous power after azimuth focusing. The profile obtained from integrating the focused signal power over range is depicted in **Figure 10**. The results present first and second orders azimuth ambiguities since $PRF \approx \frac{B_{az}}{3}$. There is also a noticeable asymmetry of the ambiguities. The reason for this is that the variation of the sensor's velocity during the flight, with respect to its nominal value, was not constant, inducing different phase errors over the synthetic aperture, which are not necessarily equally compensated during the reconstruction.

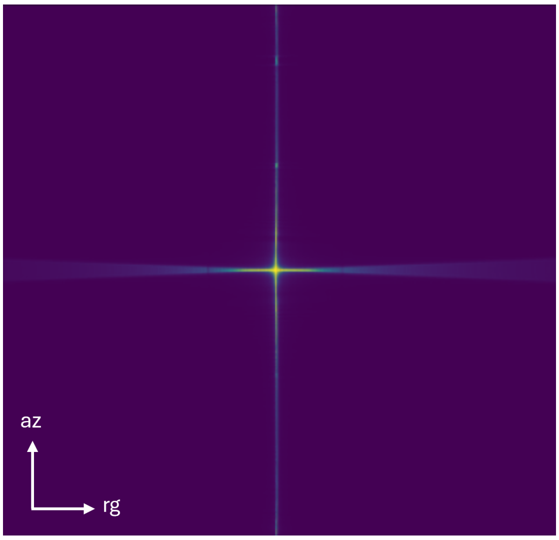

Figure 9 Focused target from the 2-D simulation with a block size of 750 samples and maximum absolute velocity variation of $0.5m/s$.

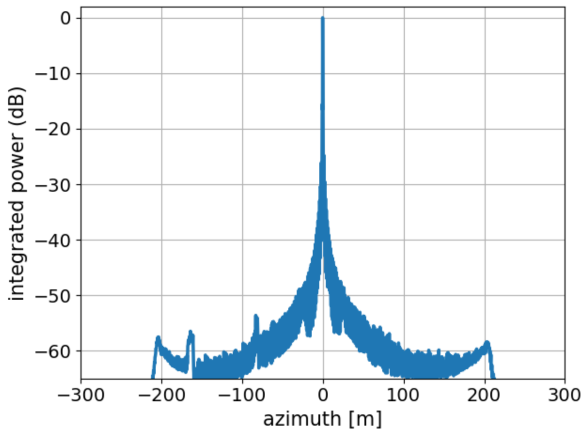

Figure 10 Profile of a focused 2-D target with block size of 750 samples and maximum absolute velocity variation of $0.5m/s$ after an integration over range.

5 Conclusions

This paper presents an analytical expression that directly relates velocity variations in a DBF SAR system to their impact on the AASR. The proposed method enables a fast and accurate initial estimation of system performance without the need for extensive simulations. The results demonstrate the potential of this approach to coherently define the optimal azimuth block size in reconstruction algorithms implementing subapertures, such as [3], by finding a suitable trade-off between ambiguity suppression and computational effort.

However, the current solution estimates the total residual ambiguous power of the range-compressed reconstructed signal and represents an upper bound of the ambiguous power after azimuth focusing. This is reflected in the results, where the ambiguity level after azimuth focusing is considerably lower than that obtained for the range-compressed signal. Therefore, the azimuth focusing steps should be incorporated into the proposed approach to achieve a more comprehensive estimation of the AASR.

Finally, the analytical solution could serve as a quality metric for a system or experiment by combining the AASR estimation proposed in [5,6] with the one introduced in this study. For this purpose, the expression presented here must be generalized to frequency intervals outside the defined reconstruction bandwidth.

6 Literature

[1] Krieger, G., Gebert, N., & Moreira, A. "Unambiguous SAR signal reconstruction from nonuniform displaced phase center sampling", in IEEE Geoscience and Remote Sensing Letters, 1(4), 2004, pp 260-264

[2] M. Davidson, N. Gebert and L. Giulicchi, "ROSE-L – The L-band SAR Mission for Copernicus," EUSAR 2021; 13th European Conf

[3] J. P. Navarro Castillo, R. Scheiber, M. Jäger and A. Moreira, "Subaperture Motion-Adaptive Reconstruction Techniques for Digital Beamforming Airborne SAR," in IEEE Transactions on Geoscience and Remote Sensing, vol. 62, 2024, pp. 1-18

[4] N. Sakar, M. Rodriguez-Cassola, P. Prats-Iraola and A. Moreira, "Azimuth Reconstruction Algorithm for Multistatic SAR Formations With Large Along-Track Baselines," in IEEE Transactions on Geoscience and Remote Sensing, vol. 58, no. 3, pp. 1931-1940, March 2020

[5] N. Gebert, G. Krieger and A. Moreira, "Digital Beamforming on Receive: Techniques and Optimization Strategies for High-Resolution Wide-Swath SAR Imaging," in IEEE Transactions on Aerospace and Electronic Systems, vol. 45, no. 2, pp. 564-592, April 2009

[6] N. Gebert, M. Villano, G. Krieger and A. Moreira, “Errata: Digital Beamforming on Receive: Techniques and Optimization Strategies for High-Resolution Wide-Swath SAR Imaging,” in IEEE Transactions on Aerospace and Electronic Systems, vol. 49, no. 3, pp. 2110-2110, July 2013.

[7] A. Reigber et al., “The High-Resolution Digital Beamforming Airborne SAR System DBFSAR,” Remote Sensing, vol. 12, no. 11, p. 1710, May 2020.

[8] A. Reigber et al., “Very-High-Resolution Airborne Synthetic Aperture Radar Imaging: Signal Processing and Applications,” Proceedings of the IEEE, vol. 101, no. 3, pp. 759–783, Mar. 2013.